Hybrid Three-Arm Coupler Consisted of Long Range Surface Plasmon Polariton and Dielectric Waveguides

Fang Liu, Ruiyuan Wan, Yi Rao, Yuxin Zheng, Yidong Huang, Wei Zhang, and Jiangde Peng

***Abstract*—The hybrid three-arm coupler, which consists of the middle long range surface plasmon polariton (LRSPP) waveguide and two outside conventional dielectric waveguides, is proposed and analyzed numerically with finite element method. The characteristics, including coupling length, coupling loss, extinction ratio and frequency dependence, are discussed in detail with different structure parameters. Compared with the two-arm hybrid coupler, the coupling loss of the three-arm hybrid coupler based devices can be reduced, especially with wider middle LRSPP waveguide. Extra transmission loss on the metal strip can be avoided because of the lossless input and output arms. Furthermore, different from conventional three-arm dielectric coupler, we find that the three-arm hybrid coupler with asymmetric structure can reach a much higher extinction ratio by introducing a middle arm offset. Since the middle arm can only transfer the TM mode from one dielectric arm to the other one within the TM mode coupling length, this structure is promising for realizing integrated polarization splitter or other functional devices.**

***Index Terms*—Hybrid coupler, long-range surface plasmon polariton (LRSPP), polarization splitter.**

I. Introduction

SURFACE Plasmon Polariton (SPP) is transverse-magnetic surface electromagnetic excitation that propagates in a wave like fashion along the metal and dielectric interface [1]. For a thin metal film, the SPP on the two interfaces couple and form the long-range surface plasmon polariton (LRSPP) mode [2], which has very low loss and can propagate longer distance than the conventional SPP. The characteristics of the LRSPP mode were analyzed carefully at the end of last century [3], [4] and its applications in sensing area were also reported [5], [6]. Furthermore, the two dimensional confined LRSPP supported by the metal strip, which is a new kind of waveguide-LRSPP waveguide with low loss, has been predicted [7] and verified experimentally [8], [9]. In recent years, LRSPP based devices, including coupler [10]–[12], modulator, switch, bragg gratings [13]–[15], and etc., have been reported and show their potential applications of integrated optical circuit because that they not only provide an approach to carry optical signals and electrical signals simultaneously [13], [16], [17], but also can be fabricated easily by using convenient planar technique. Meanwhile, the combination of the SPP with the conventional optical devices [18], [19] is worthy of expectation in the communication and sensor fields.

Both integrated plasmon-dielectric waveguides [18] and SPP-single mode dielectric waveguide polarizer [19] have shown the conversion between SPP and dielectric waveguide mode and the intention to realize integrated dielectric-plasmon circuits. However, high transmission loss of the SPP makes them impractical. We have demonstrated theoretically that the hybrid coupler, which consists of dielectric waveguide(s) and metal strip, has a high efficient coupling between LRSPP and dielectric waveguide mode with significantly reduced loss [20], [21]. Besides providing an approach to couple the signal among integrated devices and realizing polarization control, just like what was realized in the pure LRSPP coupler [10]–[12] and two-arm hybrid coupler [20], the proposed three-arm hybrid coupler has two dielectric arms for coupling to avoid the extra transmission loss on the metal strip [21]. Different from the conventional three-arm dielectric coupler [22], it is shown that the asymmetric structure for the three-arm hybrid coupler can improve the extinction ratio remarkably by introducing an offset of the middle arm. In this paper, the characteristics of the three-arm hybrid coupler with different structure parameters, including coupling length, coupling loss, extinction ratio, and frequency dependence, are discussed carefully. A guiding principle is given here for designing the three-arm hybrid couplers with required performances, fabrication tolerance and bandwidth.

The paper is organized as follows. Section II describes the structure of the three-arm hybrid coupler and the modeling method. In Section III, the simulation results are given for symmetric structure (part A), asymmetric structure (part B), and the structure with different width of middle LRSPP arm (part C). The frequency dependence of the hybrid coupler is also analyzed (part D). Section IV compares the characteristics of the three-arm hybrid coupler with the two-arm one and proposes some potential applications. In Section V, some conclusions are given.

II. Structure and Modeling Method

The proposed three-arm hybrid coupler and the coordinates are shown in Fig. 1(a). The propagation direction is along z axis. Different from the conventional three-arm dielectric coupler [22], the middle arm is replaced by a metal strip (LRSPP mode waveguide) with thickness T_m and width W_m. The two T_d thick and W_d width outside arms are the same dielectric waveguides with distance D between them. Fig. 1(b) shows the cross

Manuscript received September 27, 2007; revised June 24, 2008. Current version published January 28, 2009. This work was supported by the National Basic Research Program of China (973 Program) under Contract No. 2007CB307004.

The authors are with the State Key Laboratory of Integrated Optoelectronics, Department of Electronic Engineering, Tsinghua University, Beijing 100084, China (e-mail: liufang03@mails.tsinghua.edu.cn; wry06@mails.tsinghua.edu.cn; raoy@mails.tsinghua.edu.cn; zhengyx04@gmail.com; yidonghuang@mail.tsinghua.edu.cn; zwei@mail.tsinghua.edu.cn; pengjd@mail.tsinghua.edu.cn).

Digital Object Identifier 10.1109/JLT.2008.928397

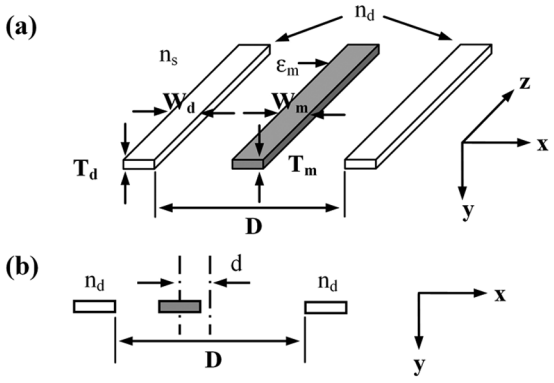

Fig. 1. (a) Parallel three-arm hybrid coupler, dark arm (middle) stands for the metal strip and white arms (left and right) stand for the dielectric waveguides. (b) The cross section of the three-arm hybrid coupler with d standing for the middle arm offset.

section of the hybrid coupler in the x-y plane, and d stands for the offset of the middle LRSPP arm. When $d = 0$, the hybrid coupler is symmetric, otherwise, it is asymmetric. Both symmetric and asymmetric structure will be discussed in Section III.

Coupled eigenmodes supported by the hybrid coupler were calculated directly to analyze the coupling characteristics among the three arms instead of solving the coupled mode equations [23]. The electromagnetic fields and propagation constants of coupled eigenmodes supported by the three-arm hybrid coupler were solved by using the software FEMLAB [24], which implements the Finite Element Method (FEM) to solve the Maxwell's equations and can be adopted to calculate the SPP mode. The energy transfer among the three arms results from the different field patterns and phase speeds [23]. Therefore, coupling of dielectric modes and LRSPP mode can be revealed by the three coupled eigenmodes.

With two single-mode dielectric waveguides and a LRSPP waveguide, the proposed hybrid coupler also has three transverse magnetic (TM) polarized eigenmodes (mode A, B, and C), similar to the conventional three dielectric waveguides coupler [22], but two transverse electric (TE) polarized eigenmodes (even and odd). This will be discussed carefully later in Section III. Discussion will be focused on TM mode here because coupling of TM mode is much stronger than that of TE mode.

It is easy to know that any TM mode supported by the hybrid coupler can also be expressed in terms of a linear superposition of eigenmodes, A, B, and C [22], [25]

$$\mathbf{H}(x,y,z) = \sum_j a_j \mathbf{H}_j(x,y) e^{i\beta_j z} \quad (j = A,B,C) \tag{1a}$$

$$\mathbf{E}(x,y,z) = \sum_j a_j \mathbf{E}_j(x,y) e^{i\beta_j z} \quad (j = A,B,C) \tag{1b}$$

where $\mathbf{H}_j$ and $\mathbf{E}_j$ are the magnetic and electric fields of eigenmode A, B, and C when $z = 0$ respectively, $\beta_j = \beta_{jr} + i \times \beta_{ji}$ are the corresponding complex propagation constants, and a_j $(j = A,B,C)$ are the corresponding mode amplitudes. Then the individual TM mode $\mathbf{H}_d$ $(\mathbf{E}_d)$ of the left or right dielectric arm is considered as the input applied on the corresponding arm [20]. With the fields normalized for all modes

$$\frac{1}{2}\int \left(\mathbf{E}_j \times \mathbf{H}_j^*\right) \cdot \overset{\triangledown}{z} dxdy = 1, \quad (j = A,B,C,d) \tag{2}$$

the amplitudes of three eigenmodes can be derived from [23]

$$a_j = \frac{1}{2}\int \left(\mathbf{E}_d \times \mathbf{H}_j^*\right) \cdot \overset{\triangledown}{z} dxdy, \quad (j = A,B,C). \tag{3}$$

Therefore, the intensity of the magnetic field supported by the three-arm hybrid coupler can be expressed as

$$\begin{aligned} &|\mathbf{H}(x,y,z)|^2 \\ &\quad = \sum_j \left[b_j \mathbf{H}_j(x,y)\right]^2 + \sum_{m,n} 2 b_m b_n \mathbf{H}_m(x,y) \\ &\qquad \times \mathbf{H}_n(x,y)\cos(\beta_{mr} - \beta_{nr}) z \\ &(b_j = a_j e^{-\beta_{ji} z},\ j,m,n = A,B,C,\ m \neq n). \end{aligned} \tag{4}$$

Similar to the conventional three-arm dielectric coupler [22], the coupling length of the hybrid coupler L_c is defined as $2\pi/(\beta_{Ar} - \beta_{Br})$. When $z = L_c$, the intensity of the magnetic field is

$$\begin{aligned} &|\mathbf{H}(x,y,L_c)|^2 \\ &\quad = \left[b_A \mathbf{H}_A(x,y) + b_B \mathbf{H}_B(x,y) - b_C \mathbf{H}_C(x,y)\right]^2 \\ &\qquad + \sum_k 2 b_k b_c \mathbf{H}_k(x,y) \mathbf{H}_c(x,y) \left[1 - \cos\left(PMF \cdot \pi\right)\right] \\ &(k = A,B) \end{aligned} \tag{5}$$

in which

$$\mathrm{PMF} = \left| \frac{\beta_{Ar} + \beta_{Br} - 2\beta_{Cr}}{\beta_{Ar} - \beta_{Br}} \right| \tag{6}$$

is the phase match factor (PMF).

The coupling loss (C.L.)

$$\mathrm{C.\,L.} = 10 \lg \left(\frac{\sum_j a_j^2}{\sum_j (a_j e^{-\beta_{ji} L_c})^2} \right), \quad (j = A,B,C) \tag{7}$$

describes the loss of the hybrid coupler at propagation distance L_c. Another important characteristic of the coupler is extinction ratio (E.R.), which is defined as the ratio of the output power from the output dielectric arm P_o and the residual power remained in the input arm P_r [23]

$$\mathrm{E.\,R.} = -10 \lg \left(\frac{P_o}{P_r} \right). \tag{8}$$

The energy proportion of each eigenmode at the input end is defined as

$$\mathrm{Energy\ Proportion} = \frac{a_j^2}{(a_A^2 + a_B^2 + a_C^2)}, \quad (j = A,B,C). \tag{9}$$

III. Simulation Results and Discussions

In the first three parts (part A, B, and C) of this section, the wavelength λ_0 is fixed at 1.55 μm to discuss the characteristics of the three-arm hybrid coupler. We assume that the two outside dielectric waveguides ($n_d = 1.54$) and the Au

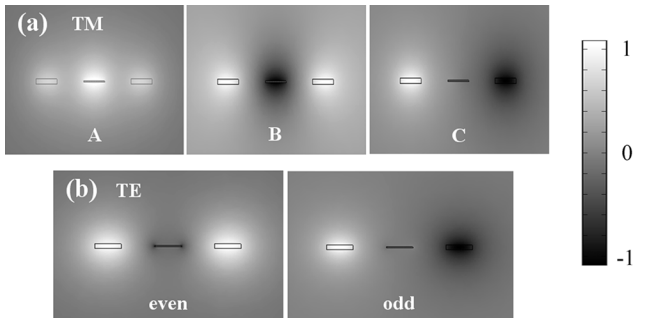

Fig. 2. (a) The H_x component of magnetic fields of three TM polarized eigenmodes supported by the hybrid coupler in the x-y plane. (b) The H_y component of magnetic fields of two TE polarized eigenmodes.

($\varepsilon_m = -132 + i \times 12.65$ at $\lambda_0 = 1.55\ \mu\mathrm{m}$) strip are surrounded by $\mathrm{SiO_2}(n_s = 1.444)$ [26]. The thickness and width of the dielectric arms are fixed at $T_d = 393\ \mathrm{nm}$ and $W_d = 2\ \mu\mathrm{m}$, respectively. With the above dielectric waveguide size, the 1/e spot sizes of the TE and TM dielectric waveguide modes are rather close to each other (about 3.5 μm). Of course, the middle LRSPP arm can have different width and thickness. In part A and B of this section, the width of the Au arm W_m is fixed at 2 μm with different thickness T_m for symmetric and asymmetric structure. In part C, W_m is also changed. Part D is devoted to the frequency dependence of the hybrid coupler.

A. Symmetric Structure

Similar to the conventional three dielectric waveguides coupler [22], the proposed hybrid coupler also has three TM polarized eigenmodes, two symmetric modes A and B, and an antisymmetric mode C. Their main component of magnetic fields (H_x) are shown in Fig. 2(a), where $D = 7\ \mu\mathrm{m}$ and $T_m = 81\ \mathrm{nm}$. For mode A, the magnetic field has the same direction in all the positions. For mode B, the field direction around the middle arm is opposite from that around outside arms. While mode C has opposite field direction around the two outside arms. T_m selected here is much thicker than that in [8] and [9]. The reason is that we look for LRSPP mode with similar size along x and y axis, and smaller metal strip width W_m corresponds to thicker metal thickness T_m [27]. An initial T_m value is around 80 nm, and finer selection of T_m should also consider the coupling efficiency and losses, which will be discussed later in the paper.

For TE polarized eigenmodes, their main component of magnetic fields (H_y) are shown in Fig. 2(b) with different situation. Only two eigenmodes, even and odd, are existent just as there is no middle LRSPP arm. This is because LRSPP mode supported by the middle arm is TM polarized [7], [8]. In principle, TE polarized electromagnetic field can also couple between two outside dielectric arms. However, without the help of the middle arm, the coupling length L_c of TE mode is two orders of magnitude larger than that of TM mode because of the comparative large distance between the two outside arms. Therefore, it can be considered that there is no coupling for TE mode within the TM coupling length and the following discussion is focused on TM mode.

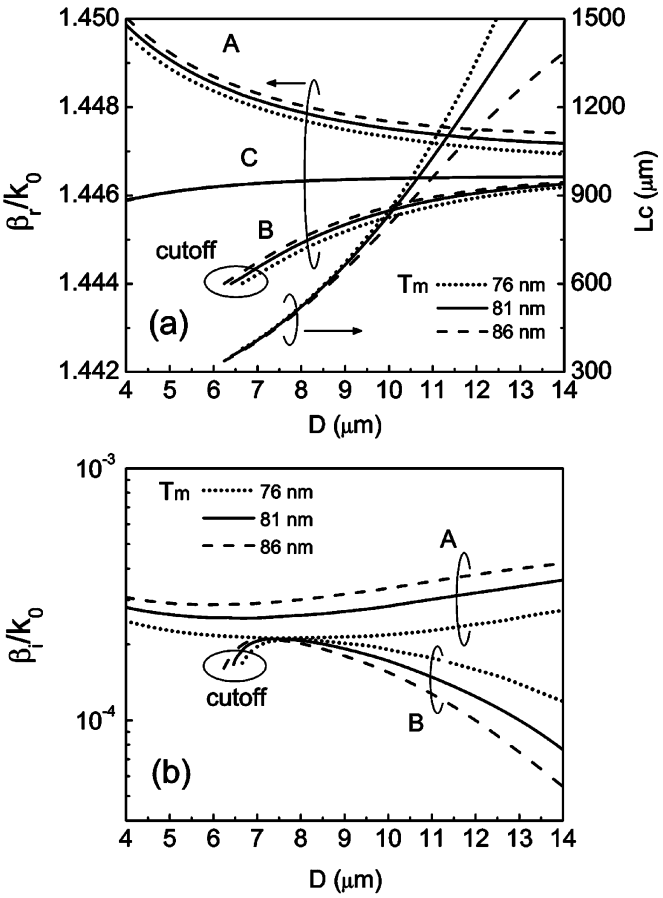

Fig. 3. (a) Effective index (β_r/k_0) and coupling length L_c versus D with $W_m = 2\ \mu\mathrm{m}$ and different T_m. Mode B is cutoff when D is small, and thinner T_m corresponds to larger cutoff distance D. (b) Normalized attenuation constants (β_i/k_0) of mode A and B with different T_m. The loss of mode C is much lower than those of mode A and B, thus it is not shown in the figure.

Fig. 3(a) shows the effective indices (β_r/k_0) of three eigenmodes and the coupling length L_c as a function of D for different LRSPP arm thickness T_m. For mode C, β_r/k_0 changes little with varying T_m. This is because there is little field surrounding the middle arm, as shown in Fig. 2(a), for mode C to feel the changes of Au strip. For mode B, cutoff occurs as arm distance D decreases, and thicker middle arm has smaller cutoff distance. Near the cutoff point, the coupling length for different T_m is rather close and shorter than 350 μm. This is of great potential for realizing compact optical components. Fig. 3(b) shows β_i/k_0 of mode A and B, which determines the propagation loss. It can be seen that, as D increases, β_i/k_0 of mode A increases while that of mode B decreases. This is because that coupling between LRSPP arm and dielectric arms becomes weaker when D increases. Therefore, mode A (B) has larger (smaller) field peak on the middle LRSPP arm with larger D. Considering the field pattern of mode C in Fig. 2(a), which has little field in the middle, it can be known why the β_i/k_0 of mode C is less than 10^{-5} and can be neglected compared with those of mode A and B.

With the eigenmodes field pattern and propagation constant, then according to (4), we can depict how TM polarized electromagnetic field couples among three arms. Taking $T_m = 81\ \mathrm{nm}$,

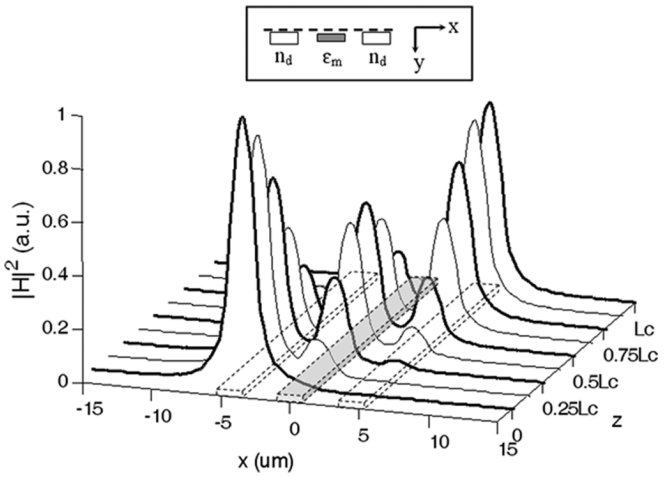

Fig. 4. Intensity of magnetic field (TM polarized) sampled along the dashed line in the inset, where $W_m = 2\ \mu\mathrm{m}$, $T_m = 81\ \mathrm{nm}$, $D = 7\ \mu\mathrm{m}$. Energy couples from left dielectric waveguide (left) to the right dielectric waveguide (right) through the LRSPP waveguide (middle) along propagation direction z. The inset shows the x-y plane cross section of the hybrid coupler and the dashed line rather near the top surface of strips.

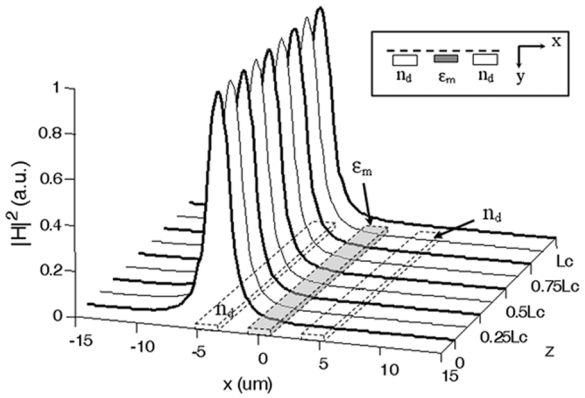

Fig. 5. Intensity of magnetic field (TE polarized) sampled along the dashed line in the inset. TE energy propagates directly through the input dielectric waveguide within the TM coupling length L_c.

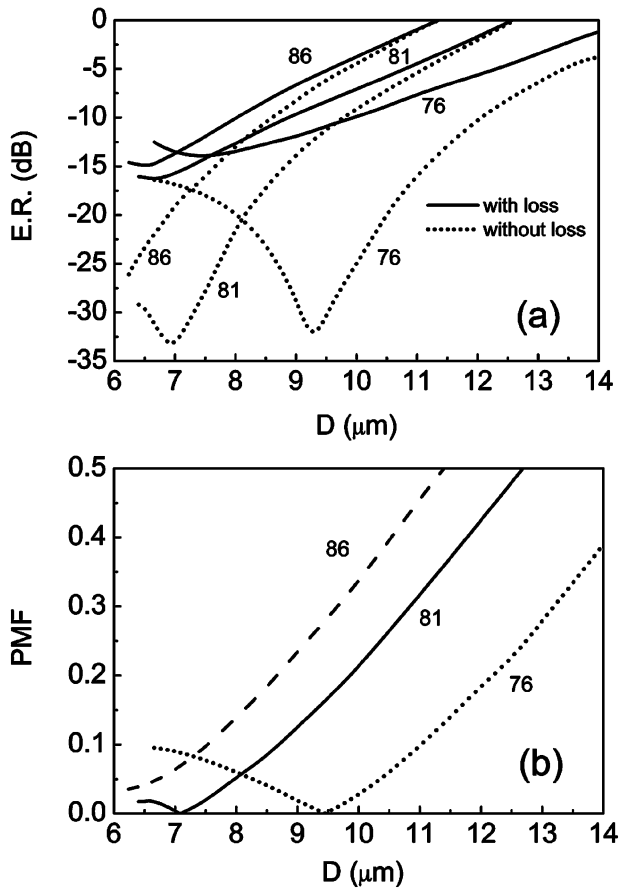

Fig. 6. (a) Extinction ratio versus D when considering eigenmode losses (solid line) or ignoring their losses (dashdotted line) with $W_m = 2\ \mu\mathrm{m}$ and $T_m = 76$, 81, 86 nm. (b) The absolute value of phase match factor (PMF) with different T_m. When ignoring the losses of eigenmdoes, the extinction ratio [dotted line in (a)] is mainly decided by PMF.

$D = 7\ \mu\mathrm{m}$ for example, Fig. 4 shows the intensity of the magnetic field along the dotted line in the inset, rather near the top surface of the strips, since LRSPP mode has its maximum field value on the surface [7]. It is shown that energy transfers gradually from the left dielectric arm to the middle LRSPP arm, then the right dielectric arm. With the same structure parameters and similar calculation method, it can be seen in Fig. 5 that TE mode propagates directly through the input arm within the TM mode coupling length.

Equation (8) describes how much energy has been coupled to the output arm. If we assume the eigenmodes are lossless ($\beta_{ji} = 0$, $j = A, B, C$), the calculated extinction ratio is shown as the dotted line in Fig. 6(a). In this case, the extinction ratio is consistent with the phase match factor (PMF) shown in Fig. 6(b), and the largest extinction ratio points correspond to the zero points of PMF. For thin LRSPP arm ($T_m = 76$, 81 nm), the largest extinction ratio near $-35\ \mathrm{dB}$ was obtained. While for thick middle arm ($T_m = 86\ \mathrm{nm}$), mode B is cutoff before reaching the largest extinction ratio point. In reality, the loss difference of the eigenmodes results in the bad extinction ratio shown by the solid line in Fig. 6(a).

According to above results, we know that there are two factors, phase match factor and loss of eigenmodes, which decide the extinction ratio of the hybrid coupler. This can also be known by analyzing (5) as follows. With considering the field pattern shown in Fig. 2(a), it is clear that the combination of mode A and B, $b_A H_A(x,y) + b_B H_B(x,y)$, forms the even mode of the two-arm coupler [12]. Mode C corresponds to the odd mode and has a phase difference π compared with the even mode. Thus the first term of (5) indicates that most of the energy has been coupled to the right dielectric arm when $z = L_c$. If eigenmodes are lossless ($a_j = b_j$, $j = A, B, C$), extinction ratio can be very high. The last two terms of (5), which are decided mainly by the phase match factor, worsen the extinction ratio. It is clear that, when $\beta_{Ar} - \beta_{Cr} \approx \beta_{Cr} - \beta_{Br}$ (PMF ≈ 0), the last two terms are rather small and high extinction ratio can be achieved, which is consistent with the conventional three-arm dielectric coupler [22].

We calculated the coupling loss (C.L.) defined by (7) and showed the results in Fig. 7(a). When D is small, it is can be seen that thinner LRSPP arm has lower coupling loss for the corresponding smaller attenuation constants of mode A shown

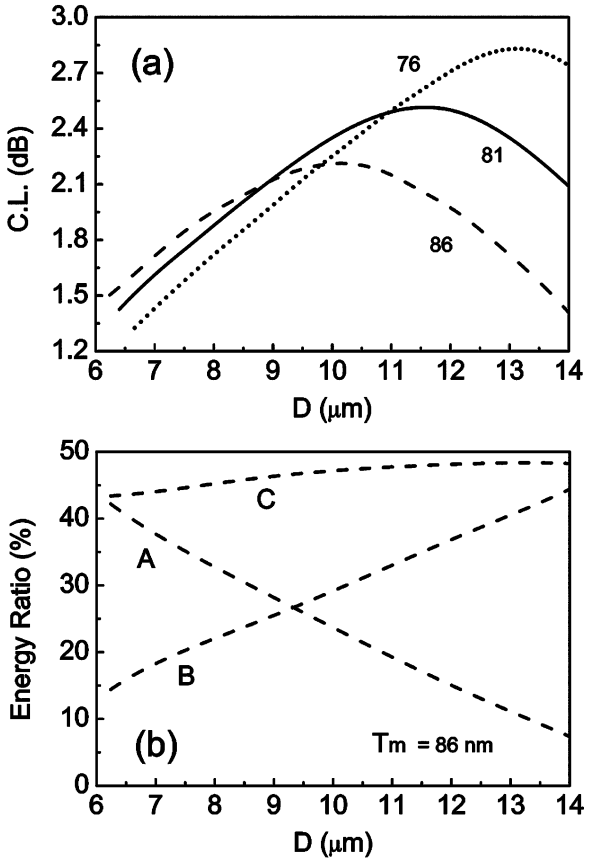

Fig. 7. (a) Coupling loss of hybrid coupler as a function of D with $W_m = 2\ \mu\mathrm{m}$ and $T_m = 76$, 81, 86 nm. (b) Taking $T_m = 86\ \mathrm{nm}$ for example, the energy proportion of the three eigenmodes defined by (9) vary with D.

in Fig. 3(b). When increasing D, it seems that the C.L. will increase quickly for increased coupling length [shown in Fig. 3(a)] according to (7). However, C.L. has the maximum value and will decrease when further increasing D. This can be explained by considering the field pattern and energy proportion of the three eigenmodes. When increasing D, mode A (B) has larger (smaller) field peak near the middle arm, and the energy guided by mode B increases as shown in Fig. 7(b). Therefore, the increased proportion of energy and decreased loss of mode B result in the decrease of coupling loss.

B. Asymmetric Structure

For conventional dielectric coupler [22], symmetric structure always has high extinction ratio. Whereas for the three-arm hybrid coupler, the symmetric structure cannot reach a high extinction ratio no matter how the structure parameters are adjusted due to the much higher loss of eigenmode A and B than that of C. Fortunately, we find that by adjusting the position of the middle LRSPP arm, the extinction ratio can be improved remarkably. This is different from the conventional three-arm dielectric coupler.

The reason why the middle arm offset is introduced to improve extinction ratio can be analyzed as follows. Eigenmodes A and B can be considered together as an even mode, like that of two-arm coupler [10]–[12], with high loss. While eigenmode C corresponds to a lossless odd mode. Fig. 8 depicts qualitatively the even (dashed line) and odd modes (dotted line) of symmetric (a) and asymmetric structure (b) to illustrate the extinction ratio of the structure. For symmetric structure, even or odd mode is symmetric or antisymmetric. Therefore, the input mode (solid line) can be decomposed to even and odd mode with equal energy at $z = 0$. After propagation distance L_c, different transmission loss of even and odd mode results in unequal energy and thus low extinction ratio [23]. On the other hand, for asymmetric structure, even and odd mode have larger peak on different sides as shown in Fig. 6(b). Therefore, to form the input, even mode should have more energy at $z = 0$. When $z = L_c$, because of larger loss for even mode, the fields of even and odd on the left side can have almost equal amplitude with a phase difference π. Therefore, high extinction ratio can be achieved with the cost of increasing even mode loss.

Fig. 9 shows the extinction ratio of the asymmetric structure with different middle arm thickness T_m. The distance between two dielectric arms, D, and the corresponding PMF value (in the bracket) when offset $d = 0$ are marked near the curve. In Fig. 9(a), T_m is fixed at 86 nm with different D. We find smaller D corresponds to higher extinction ratio. This is because that the PMF is cutoff before decreasing to zero as shown by the dashed line in Fig. 6(b), and smaller D corresponds to smaller PMF. Since PMF cannot be zero, extinction ratio can only reach $-25\ \mathrm{dB}$ when $D = 6.4\ \mu\mathrm{m}$, $d = 170\ \mathrm{nm}$.

When $T_m = 81\ \mathrm{nm}$, the PMF crosses the zero as shown by solid line in Fig. 6(b), and $D = 7\ \mu\mathrm{m}$ is near the zero point. So the solid line in Fig. 9(b) illustrates that by adjusting the position of middle LRSPP arm to $d = 170\ \mathrm{nm}$, extinction ratio as large as $-40\ \mathrm{dB}$ can be obtained. But the unsuitable D with large PMF will worsen the maximum extinction ratio. For example, the dashdotted line with $D = 6.6\ \mu\mathrm{m}$, and $\mathrm{PMF} = 1.8\%$ results in maximum $-30\ \mathrm{dB}$ extinction ratio. While for the case of $D = 8\ \mu\mathrm{m}$ (the dotted line with $\mathrm{PMF} = 5.2\%$), the maximum extinction ratio can only be $-20\ \mathrm{dB}$ with a larger offset $d = 250\ \mathrm{nm}$.

In the case of $T_m = 76\ \mathrm{nm}$, the ideal D is about 9.3 $\mu\mathrm{m}$ with $\mathrm{PMF} = 0.2\%$ according to the dotted line in Fig. 6(b). With the ideal D, the theoretical results in Fig. 9(c) show extinction ratio can be larger than $-40\ \mathrm{dB}$ when d near 290 nm. And structures with other D can not reach such high extinction ratio by adjusting offset d due to their larger PMF value. Since PMF changes little with d, the same conclusion in (a), (b), and (c) is that small PMF value of symmetric structure $(d = 0)$ corresponds to high maximum extinction ratio of asymmetric structure.

Therefore, the simulation results in Fig. 9 prove the discussions about Fig. 8. Namely, by introducing the asymmetric of the eigenmodes and utilizing their different transmission loss, high extinction ratio can be achieved by asymmetric structure. Although thin LRSPP arm ($T_m = 76\ \mathrm{nm}$ shown in Fig. 9(c)) can also reach high extinction ratio, the larger D and d means larger coupling length and coupling loss. On the other hand, thick LRSPP arm ($T_m = 86\ \mathrm{nm}$ shown in Fig. 9(a)) cannot reach high extinction ratio before cutoff. So T_m should be well selected [i.e., $T_m = 81\ \mathrm{nm}$ in Fig. 6(b)] to match the phase of three eigenmodes $(\mathrm{PMF} = 0)$ and let the corresponding D close to the cutoff point.

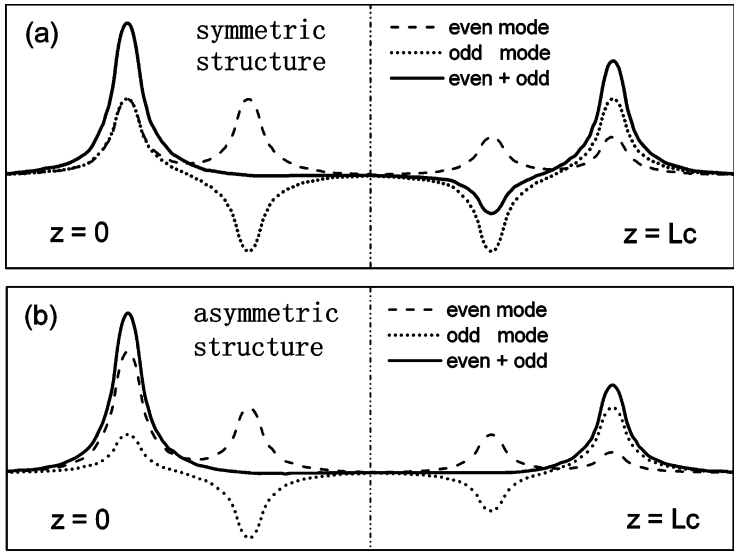

Fig. 8. Consider even and odd mode to illustrate why asymmetric three-arm hybrid coupler can reach higher extinction ratio than the symmetric. Even (dashed line), odd (dotted line) mode and their combination (solid line) when $z = 0$ and L_c for symmetric structure (a) and asymmetric structure (b).

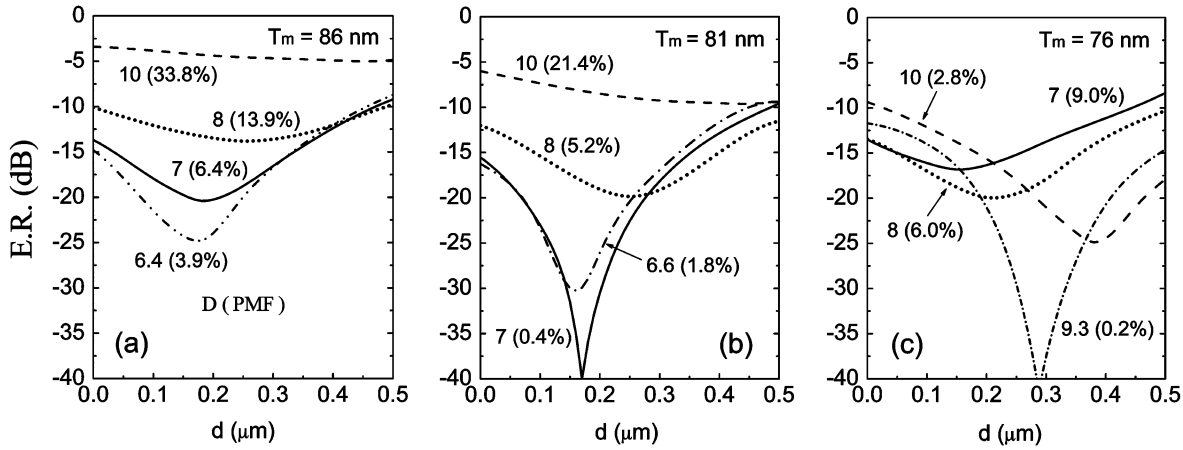

Fig. 9. Extinction Ratio of asymmetric structure with (a) $T_m = 86$ nm. (b) 81 nm. (c) 76 nm when $W_m = 2\ \mu$m. The dielectric arm distance D and the corresponding PMF value in the bracket are labeled near each curve.

From the results in Fig. 9, we can also estimate the fabrication tolerance of d, D and T_m for the three-arm hybrid coupler with the other two parameters fixed. For realizing an extinction ration of -20 dB, for example, with fixed $T_m = 81$ nm and $D = 7\ \mu$m [solid line in (b)], d has the tolerance from 70 to 270 nm. And if fix $T_m = 81$ nm and $d = 170$ nm, D will have the tolerance from 6.6 μm to near 8 μm by observing the dashdotted, solid, and dotted line. If fix $D = 7\ \mu$m, $d = 170$ nm, the tolerance of T_m may be from 78 to 86 nm when noticing the three solid lines in (a), (b), and (c).

The input is applied on the left dielectric arm when we discuss the extinction ratio of the coupler. There is no difference if input is moved to the right dielectric arm if the structure is symmetric. However, for the asymmetric structure, the asymmetric eigenmodes result in different situation. As shown in Fig. 10, with the input applied on right dielectric arm, which is equal to the case of keeping the input to the left arm and moving the middle arm to the right $(d < 0)$, the extinction ratio goes bad with increased $|d|$. Therefore, besides the increased coupling loss, asymmetric structure with $d < 0$ (middle arm moves away from the input arm) has worse extinction ratio than the symmetric case $(d = 0)$.

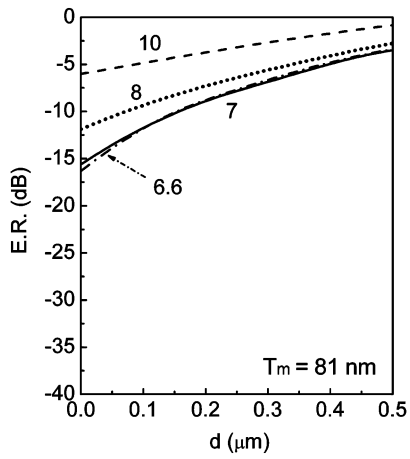

Fig. 10. When the input is applied on the right dielectric arm, the extinction ratio worsens with increased middle arm offset. Different lines correspond to different arm distance D.

We suppose this unsymmetrical feature of the extinction ratio may have some applications in special situations.

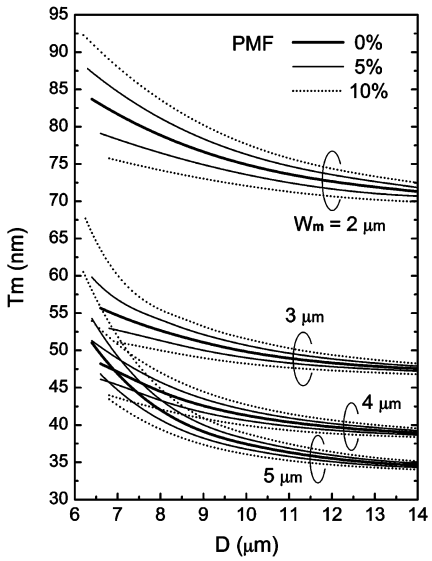

Fig. 11. The contour of phase match factor with different W_m. Within the regions between two thin sold lines of each group, the PMF value is less than 5% and can reach relative high extinction ratio.

C. LRSPP Arm With Different Width

In part A and B, the characteristics of symmetric and asymmetric structure have been analyzed with fixed width of middle LRSPP ($W_m = 2\ \mu\mathrm{m}$). In this part, the characteristics of the three-arm hybrid coupler with different middle arm width will be discussed, and it will be found that improved performance can be obtained by optimizing W_m.

The results similar to those shown in Fig. 9 can be derived with different W_m, where better (smaller) PMF also corresponds to larger maximum extinction ratio. For estimating the extinction ratio and deriving the corresponding structure parameters more simply and directly, the contour of PMF for symmetric hybrid coupler is revealed in Fig. 11. The four groups of curves correspond to $W_m = 2, 3, 4$, and 5 μm, respectively. By the way, for the metal strip design in Fig. 11, no higher order long range modes (e.g., as $^{0}_{b}$ [7]) can be supported.

According to the thick solid lines, it is known how to select T_m with different W_m to realize $\mathrm{PMF} = 0$. For example, when W_m is widened from 2 to 3 μm with $D = 7\ \mu$m, the T_m should decrease from 81 to 55 nm to match the phase and achieve high extinction ratio. If W_m changes to 4 μm, T_m can be reduced by near 50%. Results in Fig. 11 show that wider W_m corresponds to thinner T_m.

The curves in Fig. 9 have shown that, to reach an extinction ratio of -20 dB, PMF should be better (smaller) than 5%. In Fig. 11, the region between two thin solid lines of each group has PMF value better than 5% and can have high extinction ratio. With fixed dielectric arm distance D, the fabrication tolerance of T_m (ΔT_m) can be estimated. To find out the trend of ΔT_m more clearly, the exact values corresponding to the curves in Fig. 11 are listed in Table I. It is found that wider W_m corresponds to smaller ΔT_m, except the case of small D with large W_m. The exception may result from the too small distance between the dielectric arms and metal arm.

TABLE I
ΔT_m WITH PMF BETTER THAN 5% (BETWEEN THE TWO DASHED LINES OF EACH GROUP IN FIG. 11) WITH DIFFERENT D AND W_m

ΔT_m (nm)		D (μm)			
		7	9	11	13
W_m (μm)	2	6.4	3.4	2.2	1.6
	3	4.1	2.1	1.3	0.8
	4	3.5	1.83	1.11	0.7
	5	4.5	1.78	1.1	0.67

Since smaller D corresponds to shorter coupling length L_c and larger fabrication tolerance ΔT_m, as shown in Fig. 11, we fix D at 7 μm to compare the characteristics with different W_m. According to the thick solid line in Fig. 11, central T_m can be selected for $\mathrm{PMF} \approx 0$ with different $W_m = 2$, 3, 4 and 5 μm, then find out their corresponding optimized d for high extinction ratio. The extinction ratio of asymmetric structure as a function of T_m was calculated and the results are shown in Fig. 12(a). The exact fabrication tolerance ΔT_m (with E.R. better than -20 dB), which are a little larger than those in Table I, are listed in the inset table. Therefore, we cannot only get the approximate value of ΔT_m by the PMF value in Fig. 11, but also the exact value by the above method.

Fig. 12(b) and (c) illustrates the coupling length and coupling loss within the ΔT_m range shown in the inset table of Fig. 12(a). It can be seen in Fig. 12(b) that wider middle arm can shorten the coupling length. When $W_m = 2\ \mu$m, the coupling length L_c is near 400 μm. While for $W_m = 5\ \mu$m, L_c is less than 300 μm. The decrease of the coupling length should result from the closer distance between middle arm and dielectric arms with wider W_m. Commonly, shorter coupling length results in lower coupling loss according to (7). This can be seen in Fig. 12(c) when comparing the coupling loss corresponding to $W_m = 2, 3$ and 4 μm. Nevertheless, when $W_m = 5\ \mu$m, the coupling loss does not decrease continuously in spite of the shortest coupling length.

This abnormal phenomenon is due to the increased loss of mode C. For 2 μm wide middle arm, the loss of mode C is neglectable compared with those of mode A and B. When widening the middle metal strip, metal strip extends gradually into the field of mode C. As shown in Fig. 13, where $W_m = 5\ \mu$m, there exists field of mode C surrounding the metal strip and the loss of mode C cannot be neglected. Since the coupling loss is determined by both coupling length and losses of the three eigenmodes according to (7). Thus, the increased loss of mode C for $W_m = 5\ \mu$m results in the above abnormal coupling loss.

D. Frequency Dependence

The frequency dependence of the asymmetric hybrid coupler is discussed in this part. Here, we assume the refractive index of the dielectrics dose not change with the frequency (vacuum wavelength λ_0) of input light. However, noble metal Au is a kind of dispersion material and its dielectric constant changes with wavelength [26].

Taking $W_m = 2\ \mu$m for example, Fig. 14 shows how extinction ratio changes with λ_0 for different arm distance D ($= 7, 8, 9\ \mu$m) with proper middle arm thickness T_m according

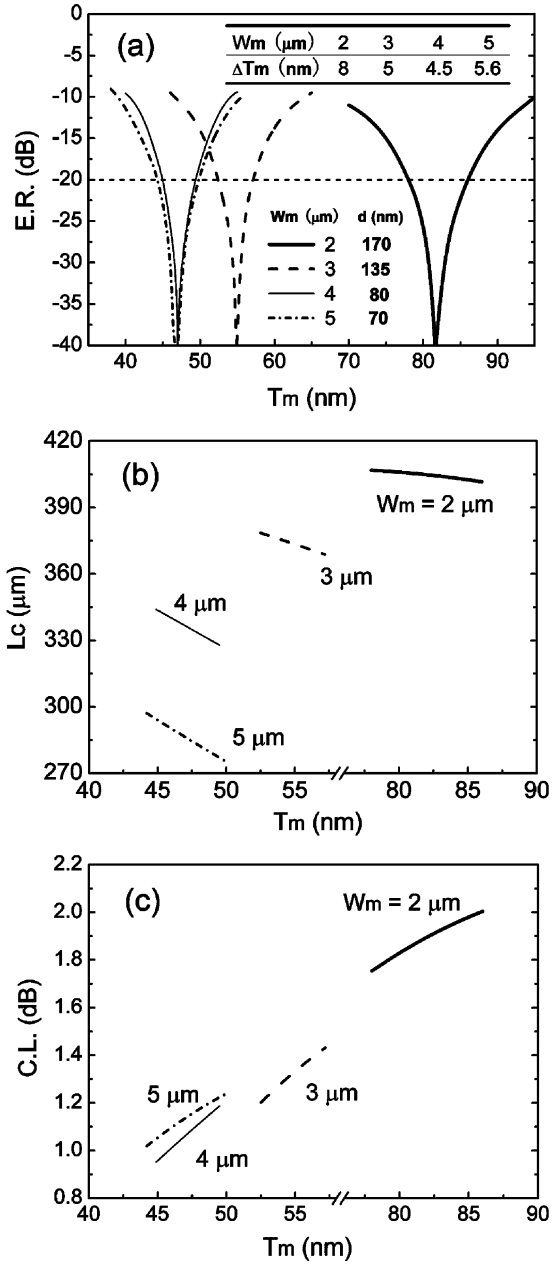

Fig. 12. (a) Extinction ratio versus middle arm thickness T_m with different W_m and corresponding d when $D = 7\ \mu\mathrm{m}$. The inset table shows the fabrication tolerance ΔT_m, within which the extinction ratio is better than -20 dB. (b) and (c) illustrate the coupling length and coupling loss with different W_m within the range of ΔT_m, respectively.

to Fig. 11. It can be seen that the bandwidth for extinction ratio higher than -20 dB is about 70–100 nm with different D. For smaller D, the cutoff of mode B is easier to occur when increasing the wavelength, while, the bandwidth for E.R. > -20 dB is larger if there is no cutoff.

Fixing the outside arm distance D at 7 μm with different middle LRSPP arm width W_m, the frequency dependence was calculated. As shown in Fig. 15, where for different W_m with selected T_m for PMF $= 0$ (thick solid line in Fig. 11) to reach high extinction ratio, it is found the bandwidth for E.R. > -20 dB can be extended to 100 nm ($W_m = 3\ \mu$m) or even 168 nm ($W_m = 5\ \mu$m) by widening the LRSPP arm width. Therefore, for smaller D and larger W_m, the hybrid coupler has larger

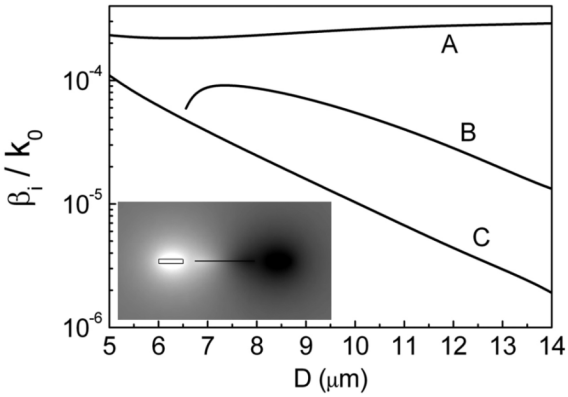

Fig. 13. Normalized attenuation constants (β_i/k_0) of the symmetric structure for three eigenmodes when $W_m = 5\ \mu$m. Field distribution of mode C in the inset indicates that the large loss results from the extending of metal strip into the field.

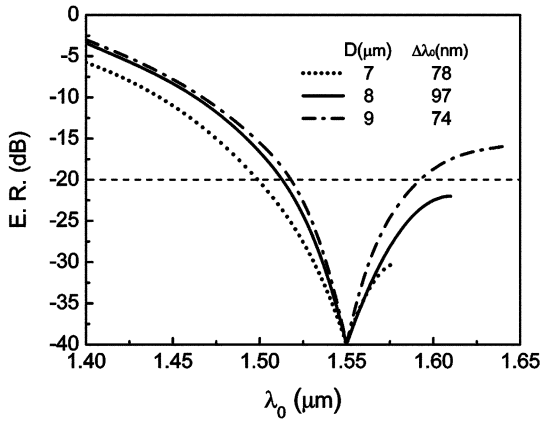

Fig. 14. Extinction ratio vs wavelength λ_0 when fix W_m at 2 μm, with $(D, T_m, d) = (7\ \mu\mathrm{m}, 82\ \mathrm{nm}, -170\ \mathrm{nm})$ (dotted line), $(D, T_m, d) = (8\ \mu\mathrm{m}, 80\ \mathrm{nm}, -225\ \mathrm{nm})$ (solid line), and $(D, T_m, d) = (9\ \mu\mathrm{m}, 77\ \mathrm{nm}, -270\ \mathrm{nm})$ (dashdotted line). The -20 dB bandwidth is shown in the inset.

bandwidth for high extinction ratio. This can be considered as the results of the smaller gap among three arms and relative stronger coupling.

The extinction ratio calculated here is all for their corresponding coupling length. Namely, for different parameters (i.e., λ_0), the coupling length is different and the extinction ratio is derived at the corresponding coupling length. For actual devices with fixed length, the extinction ratio should go bad when parameters (λ_0) changes. Fortunatelyôthe effect of the frequency change to the extinction ratio is not too large. For example, the solid line (fix $L_c = 405\ \mu$m at $\lambda_0 = 1.55\ \mu$m) in Fig. 16 is rather close to the dotted line in spite of the variation of L_c.

IV. Advantages and Applications

In this section, the characteristics of the three-arm hybrid coupler are compared with those of the two-arm hybrid coupler, and the potential applications are discussed.

In three-arm hybrid coupler, energy first couples from input dielectric arm to middle LRSPP arm and then to output dielectric arm. Its coupling length is somewhat larger than that of the

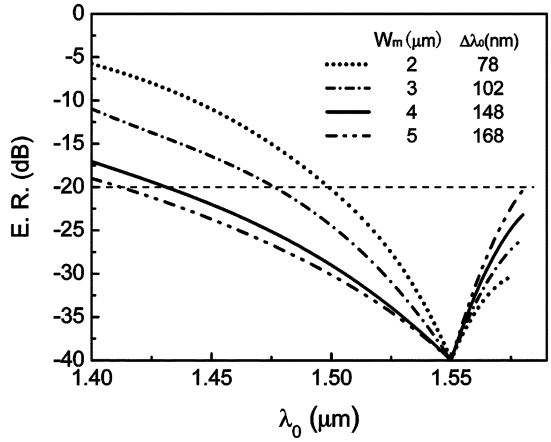

Fig. 15. Extinction ratio vs wavelength λ_0 when fix D at 7 μm, with $(W_m, T_m, d) = (2\ \mu\mathrm{m}, 82\ \mathrm{nm}, -170\ \mathrm{nm})$ (dotted line), $(W_m, T_m, d) = (3\ \mu\mathrm{m}, 55\ \mathrm{nm}, -135\ \mathrm{nm})$ (dashdotted line), $(W_m, T_m, d) = (4\ \mu\mathrm{m}, 47\ \mathrm{nm}, -100\ \mathrm{nm})$ (solid line), and $(W_m, T_m, d) = (5\ \mu\mathrm{m}, 47\ \mathrm{nm}, -70\ \mathrm{nm})$ (dash dot dot line). The -20 dB bandwidth is shown in the inset.

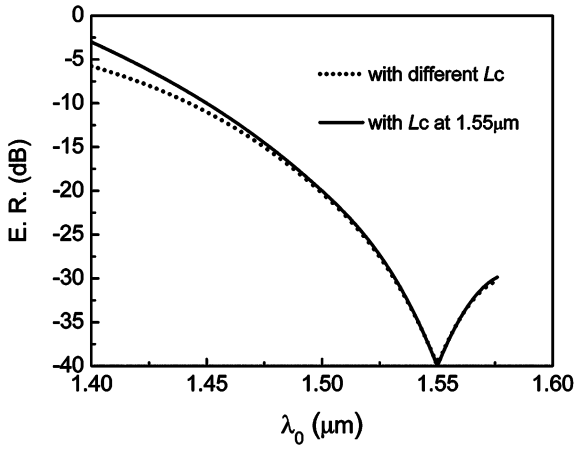

Fig. 16. Extinction ratio vs wavelength λ_0 with fixed $L_c = 405\ \mu$m at $\lambda_0 = 1.55\ \mu$m (solid line) and with different L_c (dotted line).

two-arm hybrid coupler [comparing L_c in Fig. 3(a) with the Fig. 3(b) in [20]]. With similar attenuation constants β_i/k_0 of mode A and B to those of even and odd modes of two-arm hybrid coupler, intuition may tell us that larger coupling length results in larger coupling loss. However, the reality is that three-arm hybrid coupler has lower coupling loss than that of the two-arm one [20]. Taking the symmetric three-arm structure with $D = 7\ \mu$m, $W_m = 2\ \mu$m and $T_m = 81$ nm for example, the coupling length $L_c = 408\ \mu$m and coupling loss is 1.62 dB. While for the two-arm hybrid coupler, with corresponding arm distance of 2.5 μm, the coupling length L_c is 308 μm and coupling loss is 1.82 dB [20]. The reason is that, in the case of three-arm hybrid coupler, near half of the energy is guided by mode C with very low loss. From Fig. 12(b) and (c), it can be seen that the coupling length and loss can be further reduced by widening the middle LRSPP arm. More importantly, for two-arm hybrid coupler, TM light coupled to LRSPP arm guided by the Au strip with comparative high loss. Therefore, the total loss of the two-arm coupler includes not only the coupling loss within the coupling length but also the extra transmission loss on the metal strip. However, in the three-arm coupler, the right lossless dielectric arm guides the TM light at last and all of the losses only result from the coupling loss.

In Section III, we have discussed that, without the help of middle LRSPP arm, the distance between the two outside arms is too large for TE mode coupling compared with TM mode. It can be considered that there is almost no coupling for TE mode within the TM coupling length. Thus, TE and TM mode can be separated with high extinction ratio at proper coupling length.

For the conventional polarization splitter, whose coupling length of one polarized mode is twice that of the other polarized mode [28], [29], the unsuitable structure parameters would affect the extinction ratio of the two kinds of polarization modes. While based on this hybrid coupler, the output mode from the right arm is pure TM polarized light due to too large L_c difference between TM and TE mode. The structure parameters will only decide the residual TM light in the input dielectric arm and the purity of TE mode. Compared with the splitter with ARROW structure [30] and bragg reflector waveguides structure [31], the proposed polarization splitter with hybrid coupler has the advantages of compact and simple structure. Further more, when signals are applied on the metal arm, it has the potential to easily control the TM mode coupling efficiency by electric signals, while TE mode is not affected.

With the characteristic of supporting the optical and electric signals simultaneously by the middle LRSPP arm [13], [16], electric controlled polarization combiner, modulators, and switches may also be realized based on this three-arm hybrid coupler.

V. Conclusion

We have investigated numerically the high efficiency coupling of TM mode on the three-arm hybrid coupler, which is consisted of middle LRSPP waveguide and two outside dielectric waveguides. Different from the conventional three-arm dielectric coupler, we find that symmetric structure cannot reach high extinction ratio no matter how parameters are adjusted, while asymmetric structure can reach a much higher extinction ratio (as large as -40 dB) by selecting a suitable middle arm offset.

When the three arms have the same width, the three-arm hybrid coupler has the similar coupling loss with that of the two-arm hybrid coupler. While, extra transmission loss on the metal strip can be avoided in the three-arm one because of the lossless input and output arms. Furthermore, by widening the middle arm, the coupling length and coupling loss can be shortened and reduced. However, since wider middle arm corresponds to smaller thickness fabrication tolerance, the characteristics of the coupler (coupling length, loss and metal strip thickness) and fabrication tolerance should be considered comprehensively. The frequency dependence of the three-arm hybrid coupler is also investigated and shows the relationship between the bandwidth and the structure parameters.

Since the coupling of TE mode can be neglected within the TM mode coupling length, pure TM mode is derived from the output dielectric arm. Therefore, the three-arm hybrid coupler is promising for realizing high performance TE/TM mode splitter or combiner. By applying electric signals on the middle LRSPP

arm, electric controlled polarization splitter/combiner, modulators and switches may also be realized.

ACKNOWLEDGMENT

The authors would like to thank D. Ohnishi, H. Takasu, and A. Kamisawa of ROHM Corporation for their valuable discussions and helpful comments.

REFERENCES

[1] A. V. Zayats, I. I. Smolyaninov, and A. A. Maradudin, "Nano-optics of surface plasmon polaritons," *Phys. Rep.*, vol. 408, pp. 131–314, 2005.
[2] D. Sarid, "Long-range surface-plasma waves on very thin metal films," *Phys. Rev. Lett.*, vol. 47, no. 26, pp. 1927–1930, 1981.
[3] J. J. Burke, G. I. Stegeman, and T. Tamir, "Surface-polariton-like waves guided by thin, lossy metal films," *Phys. Rev. B*, vol. 33, no. 8, pp. 5186–5201, 1986.
[4] F. Yang, J. R. Sambles, and G. W. Bradberry, "Long-range surface modes supported by thin films," *Phys. Rev. B*, vol. 44, no. 11, pp. 5855–5872, 1991.
[5] J. Ctyroky, J. Homola, P. V. Lambeck, S. Musa, H. J. W. M. Hoekstra, R. D. Harris, J. S. Wilkinson, B. Usievich, and N. M. Lyndin, "Theory and modelling of optical waveguide sensors utilising surface plasmon resonance," *Sens. Actuators B*, vol. 54, pp. 66–73, 1999.
[6] G. G. Nenninger, P. Tobiska, J. Homola, and S. S. Yee, "Long-range surface plasmons for high-resolution surface plasmon resonance sensors," *Sens. Actuators B*, vol. 74, pp. 145–151, 2001.
[7] P. Berini, "Plasmon-polariton waves guided by thin lossy metal films of finite width: Bound modes of symmetric structures," *Phys. Rev. B*, vol. 61, pp. 10484–10503, 2000.
[8] R. Charbonneau, P. Berini, E. Berolo, and E. Lisicka, "Experimental observation of plasmon-polariton waves supported by a thin metal film of finite width," *Opt. Lett.*, vol. 25, pp. 844–846, 2000.
[9] T. Nikolajsen, K. Leosson, I. Salakhutdinov, and S. I. Bozhevolnyi, "Polymer-based surface-plasmon-polariton stripe waveguides at telecommunication wavelengths," *Appl. Phys. Lett.*, vol. 82, p. 668, 2003.
[10] R. Charbonneau, C. Scales, I. Breukelaar, S. Fafard, N. Lahoud, G. Mattiussi, and P. Berini, "Passive integrated optics elements based on long-range surface plasmon polaritons," *J. Lightw. Technol.*, vol. 24, no. 1, pp. 477–494, Jan. 2006.
[11] A. Boltasseva, T. Nikolajsen, K. Leosson, K. Kjaer, M. S. Larsen, and S. I. Bozhevolnyi, "Integrated optical components utilizing long-range surface plasmon polaritons," *J. Lightw. Technol.*, vol. 23, no. 1, pp. 413–422, Jan. 2005.
[12] H. S. Won, K. C. Kim, S. H. Song, C. H. Oh, P. S. Kim, S. Park, and S. I. Kim, "Vertical coupling of long-range surface plasmon polaritons," *Appl. Phys. Lett.*, vol. 88, p. 011110, 2006.
[13] T. Nikolajsen, K. Leosson, and S. I. Bozhevolnyi, "Surface plasmon polariton based modulators and switches operating at telecom wavelengths," *Appl. Phys. Lett.*, vol. 85, pp. 5833–5836, 2004.
[14] S. Jetté-Charbonneau and P. Berini, "Theoretical performance of Bragg gratings based on long-range surface plasmon-polariton waveguides," *J. Opt. Soc. Amer. A*, vol. 23, no. 7, pp. 1757–1767, 2006.
[15] A. Boltasseva, S. I. Bozhevolnyi, T. Nikolajsen, and K. Leosson, "Compact Bragg gratings for long-rang surface plasmon polaritons," *J. Lightw. Technol.*, vol. 24, no. 2, pp. 912–918, Feb. 2006.
[16] S. I. Bozhevolnyi, T. Nikolajsen, and K. Leosson, "Integrated power monitor for long-range surface plasmon polaritons," *Opt. Commun.*, vol. 255, pp. 51–56, 2005.
[17] G. Gagnon, N. Lahoud, G. A. Mattiussi, and P. Berini, "Thermally activated variable attenuation of long-range surface plasmon-polariton waves," *J. Lightw. Technol.*, vol. 24, no. 11, pp. 4391–4402, Nov. 2006.
[18] M. Hochberg, T. Baehr-Jones, C. Walker, and A. Scherer, "Integrated plasmon and dielectric waveguides," *Opt. Express*, vol. 12, no. 22, pp. 5481–5486, 2004.
[19] P. S. Davids, B. A. Block, and K. C. Cadien, "Surface plasmon polarization filtering in a single mode dielectric waveguide," *Opt. Express*, vol. 13, no. 18, pp. 7063–7069, 2005.
[20] F. Liu, Y. Rao, Y. Huang, W. Zhang, and J. Peng, "Coupling between long range surface plasmon polariton mode and dielectric waveguide mode," *Appl. Phys. Lett.*, vol. 90, p. 141101, 2007.
[21] F. Liu, Y. Rao, X. Tang, R. Wan, Y. Huang, W. Zhang, and J. Peng, "Hybrid three-arm coupler with long range surface plasmon polariton and dielectric waveguides," *Appl. Phys. Lett.*, vol. 90, p. 241120, 2007.
[22] J. P. Donnelly, H. A. Haus, and N. Whitaker, "Symmetric three-guide optical coupler with nonidentical center and outside guides," *IEEE J. Quantum Electron.*, vol. QE-23, no. 4, pp. 401–406, Apr. 1987.
[23] W. P. Huang, "Coupled-mode theory for optical waveguides: An overview," *J. Opt. Soc. Amer. A*, vol. 11, no. 3, pp. 963–983, 1994.
[24] *"FEMLAB Electromagnetics Module Manual,"* 3.0 ed. COMSOL AB, Sweden, 2003.
[25] K. Okamoto, *Fundamentals of Optical Waveguides*. New York: Academic, 2000.
[26] E. D. Palik, *Handbook of Optical Constants of Solids*. Orlando, FL: Academic, 1985, pp. 286–297.
[27] K. Leosson, T. Nikolajsen, A. Boltasseva, and S. I. Bozhevolnyi, "Long-range surface plasmon polariton nanowire waveguides for device applications," *Opt. Express*, vol. 14, no. 1, pp. 314–319, 2006.
[28] M. Rajarajan, C. Themistos, B. M. A. Rahman, and K. T. V. Grattan, "Characterization of metal-clad TE/TM mode splitters using the finite element method," *J. Lightw. Technol.*, vol. 15, no. 12, pp. 2264–2269, Dec. 1997.
[29] I. Kiyat, A. Aydinli, and N. Dagli, "A compact silicon-on-insulator polarization splitter," *Photon. Technol. Lett.*, vol. 17, no. 1, pp. 100–102, Jan. 2005.
[30] Y. T. Huang, C. H. Jang, S. H. Hsu, and J. J. Deng, "Antiresonant reflecting optical waveguides polarization beam splitters," *J. Lightw. Technol.*, vol. 24, no. 9, pp. 3553–3560, Sep. 2006.
[31] E. Simova and I. Golub, "Polarization splitter/combiner in high index contrast Bragg reflector waveguides," *Opt. Express*, vol. 11, no. 25, pp. 3425–3430, 2003.

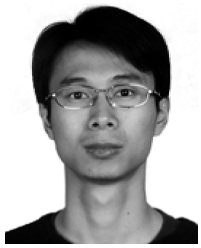

Fang Liu received the B.S. degree from Beijing Institute of Technology, Beijing, China, in 2003. He received the Ph.D. degree from the Department of Electrical Engineering, Tsinghua University, Beijing, in 2008.

His current research interest is in the area of surface plasmon polariton-based integrated optical devices and nanostructure optoelectronics.

Ruiyuan Wan received the B.S. degree from Beijing JiaoTong University, Beijing, China, in 2006. She is pursuing the Ph.D. degree at the Department of Electronic Engineering, Tsinghua University, Beijing.

Yi Rao received the B.S. and Master degrees from the Department of Electrical Engineering, Tsinghua University, Beijing, China, in 2005 and 2008, respectively. He is pursuing the Ph.D. degree at the Department of Electrical Engineering and Computer Sciences, University of California, Berkeley.

Yuxin Zheng, photograph and biography not available at the time of publication.

Yidong Huang received the B.S. and Ph.D. degrees in optoelectronics from Tsinghua University, Beijing, China, in 1988 and 1994, respectively.

From 1991 to 1993, she was with Arai Laboratories, Tokyo Institute of Technology, Japan, on leave from Tsinghua University. She was with the Photonic and Wireless Devices Research Laboratories, NEC Corporation, from 1994 to 2003, where she was engaged in the research on semiconductor laser diodes for optical-fiber communication. In 2003, she joined the Department of Electronics Engineering, Tsinghua University, as a Professor. She is presently engaged in research on nanostructure optoelectronics.

Wei Zhang received the B.S. and Ph.D. degrees from the Department of Electrical Engineering, Tsinghua University, Beijing, China, in 1998 and 2003, respectively.

In 2003, he joined the Department of Electronics Engineering, Tsinghua University, where he is currently an Associate Professor. His major research interests include active and passive fiber device, microstructure optoelectrical materials, especially microstructure fibers, and their applications.

Jiangde Peng graduated from Tsinghua University, Beijing, China, in 1964.

Since then, he has been with the Department of Electronic Engineering at the university, where he is currently a Professor. He was a Senior Visiting Scholar at CNRS Laboratoire de Photophysique Moleculare, Universite d'Orsay, France from 1973 to 1975, and in the Department of EE-Systems, University of Southern California, Los Angeles, from 1997 to 1998. He has been engaged in research on active and passive fiber devices for WDM optical fiber communications, with specific emphasis on fiber amplifiers and lasers. At present, his primary interests focus on slow light, entangled photon-pair sources, and sensors based on micro- and nanostructure materials. He received the National Invention Award in 1997. He is author or coauthor of over 100 papers, 12 patents, and the textbook *Fundamentals of Optoelectronic Technologies* (Tsinghua University Press, 1988).

Prof. Peng is a member of the Optical Society of China and SPIE.